machines

Article

# Study on Cage Wear of Railway Traction Motor Bearings Based on Analysis of Rolling Element Motion

**Daisuke Suzuki [1,*], Ken Takahashi [1], Fumihiro Itoigawa [2] and Satoru Maegawa [2]**

[1] Material Technology Division, Railway Technical Research Institute, Kokubunji 185-8540, Japan
[2] Department of Electrical and Mechanical Engineering, Nagoya Institute of Technology, Nagoya 466-8555, Japan
* Correspondence: suzuki.daisuke.83@rtri.or.jp

**Abstract:** Cylindrical roller bearings used in traction motors for railway vehicles are used at high rotational speeds and under light loads. Under these operating conditions, the life due to cage wear is much shorter than the life due to raceway fatigue. Therefore, bearing life can be extended by reducing cage wear. The authors thought that to reduce cage wear, it is necessary to establish a dynamic analysis method for the contact between the roller and the cage, and to identify the wear mode of the cage. If cage wear follows Archard's equation, then cage wear is proportional to the impulse caused by the contact between the rollers and the cage. Therefore, in this paper, a simple model consisting only of a roller and a cage was constructed, and the impulse was obtained via dynamic analysis. The impulses calculated by the dynamic analysis were in good agreement with those measured. In addition, the experiments showed that cage wear is proportional to the impulse and revealed the wear mode of the cage. These allow the method proposed in this paper to be used to predict cage wear and to determine bearing specifications to reduce cage wear.

**Keywords:** bearing; cage wear; contact force between roller and cage; impulse caused by contact between roller and cage

check for updates

**Citation:** Suzuki, D.; Takahashi, K.; Itoigawa, F.; Maegawa, S. Study on Cage Wear of Railway Traction Motor Bearings Based on Analysis of Rolling Element Motion. *Machines* **2023**, *11*, 594. https://doi.org/10.3390/machines11060594

Academic Editor: Sheng Li

Received: 28 April 2023
Revised: 21 May 2023
Accepted: 24 May 2023
Published: 30 May 2023



## 1. Introduction

It is known that cage wear becomes more significant when rolling bearings are used at high rotational speeds. Anderson et al. measured the weight loss of each component of a cylindrical roller bearing after testing at high rotational speeds and showed that cage wear is significant under these conditions [1]. To reduce cage wear, the silver plating of cages has been proposed with some success [2], but its application is limited in terms of cost. Since there is no perfect way to reduce cage wear, several studies on cage wear have been conducted to date. There are various approaches to addressing cage wear, such as examining cage specifications [3], improving lubrication [4], developing wear detection techniques [5,6], and developing cageless bearings [7]. The problem of cage wear becomes even more apparent when the bearing is used under light loads in addition to high rotational speeds. This is because, under these operation conditions, the life due to the wear of the cage is much shorter than the life due to the fatigue of the raceway. Cylindrical roller bearings used in traction motors for railway vehicles are an example of this operating condition. These bearings are used at a maximum rotational speed of approximately 6000 rpm and a load of a few percent of the basic dynamic load rating. Therefore, the bearings have to be replaced much earlier than the calculated life proposed by Lundberg and Palmgren [8]. Under these conditions of use, bearing life can be extended by reducing cage wear. Assuming a rolling element guiding cage, wear occurs at the contact area between the rolling elements and the cage. Therefore, the first step in reducing cage wear is to identify the contact conditions between the rolling elements and the cage. It is then necessary to clarify what mode of cage wear progresses under those contact conditions.

Various studies have been conducted to identify the contact conditions between rolling elements and a cage. Kakuta [9] and Stacke et al. [10] measured the contact force between a rolling element and a cage by experimentation. In both experiments, however, there was concern that constructing a mechanism to measure the contact force in the bearing would inhibit the movement of the cage. It is known that the whirl of the cage varies with rotational speed [11,12]. Since the contact force is determined by the mutual dynamics of the rolling element and the cage, restraining the movement of the cage could affect the contact force. Gupta [13–16] and Sakaguchi et al. [17,18] used a dynamic simulation to determine the contact force between the rolling element and the cage. However, the contact force obtained from simulation results was not compared with those obtained from actual measurements. In addition, these studies calculate the motion of all parts of the bearing: the inner ring, outer ring, rolling elements, and cage. In particular, a cage must be modeled as an elastic body to accurately determine the contact force [19,20]. As such, they require complex computational models and significant computational costs.

The authors measured the contact force between a rolling element and a cage using an experiment [21]. Here, a measurement system was constructed that did not interfere with the movement of the cage. In this measurement system, small load cells were attached to the cage to measure the contact force. A special mechanism was created to take the load cell cable out into a stationary field while the cage was rotating. As a result, the contact force could be measured without constraining the motion of the cage, since no tension was exerted on these cables. The measurements showed that the contact force is intermittent. The paper also showed that, if cage wear follows Archard's equation [22], the volume of wear is proportional to the impulse caused by the contact. It should be noted that in solid-lubricated cages, it has been suggested that the wear follows Archard's equation [23,24]. Therefore, the measured contact force was integrated to obtain the impulse and related to the volume of wear. According to this, only the impulse, not the contact force, is required to determine the volume of cage wear. Therefore, a simple model consisting only of the rolling element and the cage was constructed and a dynamic analysis was performed to obtain the impulse. As a result, under certain conditions, the calculation results based on the dynamic analysis agreed with the experimental results. In this dynamic analysis, the impulse is determined from the change in momentum before and after the contact, so there is no need to discuss the contact time. For the purpose of determining cage wear, this dynamic analysis is reasonable.

Estimating cage wear based on the above dynamic analysis can be an effective tool in determining operating conditions and making designs for cage life extension. However, there are two issues that must be improved from the previous paper in order to achieve this. The first issue is to improve the accuracy of the dynamic analysis. In the previous paper, the accuracy of the dynamic analysis was sufficient for high-rotational-speed conditions, but insufficient for low-rotational-speed conditions, and it deviated from the experimental results. The second issue is the verification of the assumed wear mode. In the previous paper, cage wear was assumed to be proportional to the impulse; however, this validity has not been verified. The purpose of this paper is to address these two issues and then discuss cage wear based on a dynamic analysis of rolling element motion.

## 2. Materials and Methods

### *2.1. Target Bearing*

In this paper, cylindrical roller bearings used in traction motors for railway vehicles with the specifications shown in Table 1 were targeted. Although this bearing is for railway vehicles, its specifications are almost the same as those of commercially available bearings. The raceways and rollers are made of bearing steel and the cage is made of high-strength brass. The cage is guided by rollers and has no contact except with the rollers. In other words, no force acts on the cage from the inner or outer rings.

**Table 1.** Target bearing specifications.

| Bearing Type | | Cylindrical Roller Bearing |
|---|---|---|
| Bearing number | | NU214 |
| Inner diameter | | 70 mm |
| Outer diameter | | 125 mm |
| Width | | 24 mm |
| Radial clearance | | 0.090–0.125 mm |
| Pitch circle diameter of roller $2r_p$ | | 97.5 mm |
| Number of rollers | | 16 |
| Roller diameter $2r_r$ | | 13 mm |
| Length of roller | | 13 mm |
| Mass of roller $m$ | | 13 g |
| Cage guide | | By rollers |
| Material | Race rings Rollers | Bearing steel |
| | Cage | High-strength brass |
| Basic dynamic load rating | | 83,500 N |

### *2.2. Method for Measuring Contact Force between Roller and Cage*

In one of the cage pockets, as shown in Figure 1, $F_{acc}$ which is the force to accelerate the cage acts in the front of the cage pocket and $F_{dec}$ which is the force to decelerate the cage acts in the rear of the cage pocket. These contact forces $F_c$ ($F_{acc}$ and $F_{dec}$) cause cage wear because the material of the cage is softer than that of the roller. Since $F_c$ are generated by the mutual motion of the roller and the cage, a measurement system for $F_c$ that does not interfere with the motion of the cage was constructed as shown in Figure 2. $F_c$ were measured using small load cells attached to the cage pocket. The curved surfaces of the cage pocket were machined flat to mount the load cells. Here, the distance between the load cells was adjusted to match the diameter of the cage pocket. A rotor synchronized with the rotational speed of the cage was placed in front of the test bearing. The cables of the load cells were taken out through the rotor into a stationary field so that their tension did not interfere with the movement of the cage. Note that these cables were sufficiently lightweight that the gravity and centrifugal forces acting on them were negligible. Using this measurement system, $F_c$ were measured under the conditions shown in Table 2. The rotational speed of the inner ring $n_i$ was set to a maximum of 4000 rpm. The maximum rotational speed of the target traction motor is about 6000 rpm, but due to the limitation of synchronizing the rotor with the cage, it was set at 4000 rpm. The radial load was 970 N with reference to the mass of the rotor of the traction motor.

**Table 2.** Measurement conditions.

| | |
|---|---|
| Rotational speed of inner ring $n_i$ | 500, 1000, 2000, 3000, 4000 rpm |
| Direction of rotation | Forward, reverse |
| Radial load | 970 N |
| Lubricant | Lithium complex soap grease |

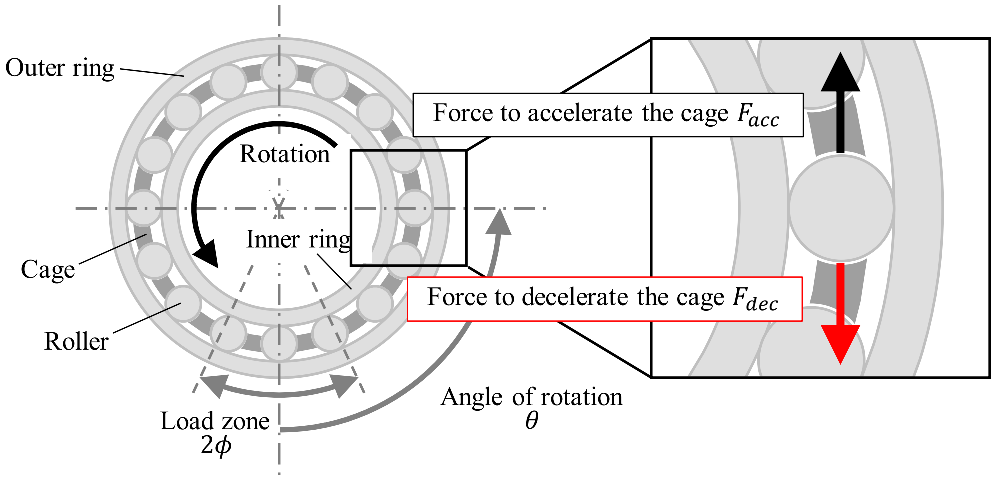


**Figure 1.** Forces acting on cage from roller.

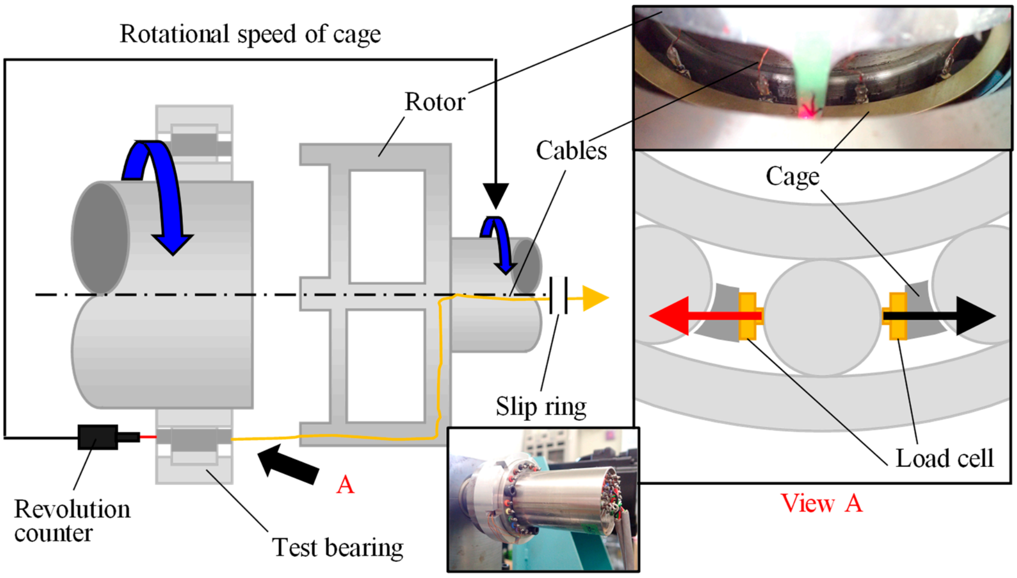


**Figure 2.** Measurement system of contact force between roller and cage.

*2.3. Method for Dynamic Analysis for Determining Impulse*

In the introduction, it was mentioned that cage wear is proportional to the impulse caused by the contact between the roller and the cage $I_c$. If $I_c$ can be determined without measurement, it will be an effective tool for the design of bearings to reduce cage wear. Based on this, in a previous paper [21], a simple model consisting of a roller and a cage was created, and a method for determining $I_c$ was presented. However, this analysis was not always sufficiently accurate. At low rotational speeds (below 1000 rpm), the measurement results and the calculation results based on the dynamic analysis did not match. In this paper, a method to obtain $I_c$ with high accuracy is proposed by improving this method. Specifically, "the gravity acting on the rollers" and "the interaction between the roller and the cage when they are at the same speed" are newly considered. As will be discussed in Section 3.1, if $n_i$ is the same, the $I_{acc}$ (impulse caused by $F_{acc}$) and $I_{dec}$ (impulse caused by $F_{dec}$) per cage rotation are approximately equal. Therefore, it is sufficient to determine one of them. In this paper, as in the previous paper, $I_{dec}$ per cage rotation occurring in the no-load zone was obtained. The following assumptions were made in creating the model.

I. Only the translational velocity of the roller changes when the roller and the cage make contact (the angular velocity of the cage $\omega_c$ is constant at a geometrically determined value.).
II. In the no-load zone, the roller contacts the outer ring raceway due to centrifugal force and does not contact the inner ring raceway.
III. The rotational speed of rollers is assumed to be constant at a theoretical value (The angular velocity of the roller $\omega_r$ is constant at a geometrically determined value.).

Under the above assumptions, consider the forces acting on the roller in the no-load zone, as shown in Figure 3. In the figure, the force in the rotational direction of the cage on the roller at a position rotated by $\theta$ is shown. The tangential force of gravity and the pressure force exerted by the oil film between the roller and the outer ring $F_o$ act on the roller. $F_{dec}$ also acts on the roller when it is in contact with the cage.

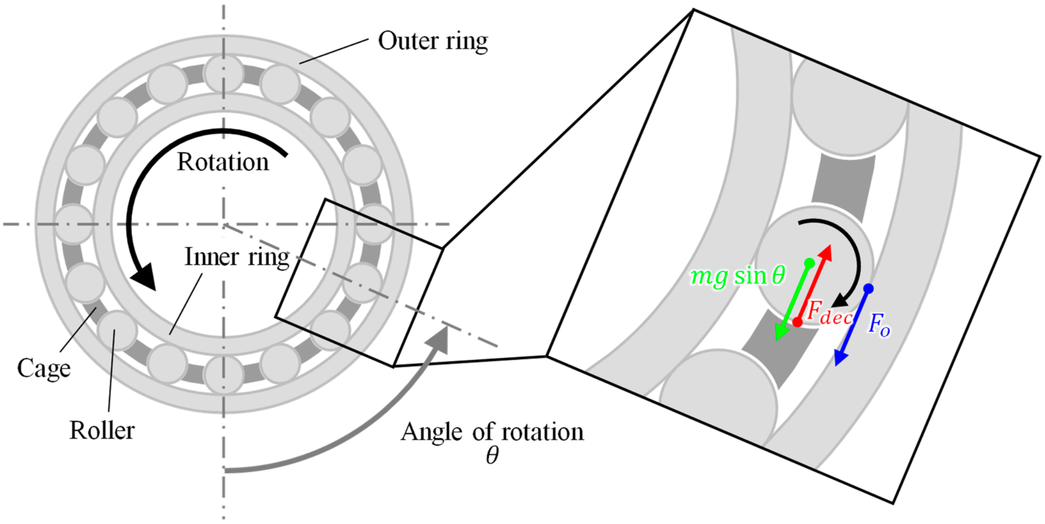


**Figure 3.** Force acting on roller (in direction of rotation of cage).

Consider the motion of the roller in the cage pocket when the force shown in Figure 3 is applied. As shown in Figure 4, in the no-load zone, the rollers are in motion in the cage pockets. Each of these steps is described below.

(1) The roller within the no-load zone is located in the front of the cage pocket. This is because the roller accelerates the cage within the loading zone.
(2) The orbital velocity of the roller is decelerated by $F_o$ and the tangential force of gravity. This causes the roller to move to the rear of the cage pocket. $F_o$ is generated by the oil film between the roller and the outer ring.
(3) The roller contacts the rear of the cage pocket. $F_{dec}$ is generated by the contact.
(4) The roller bounces and moves to the front of the cage pocket.

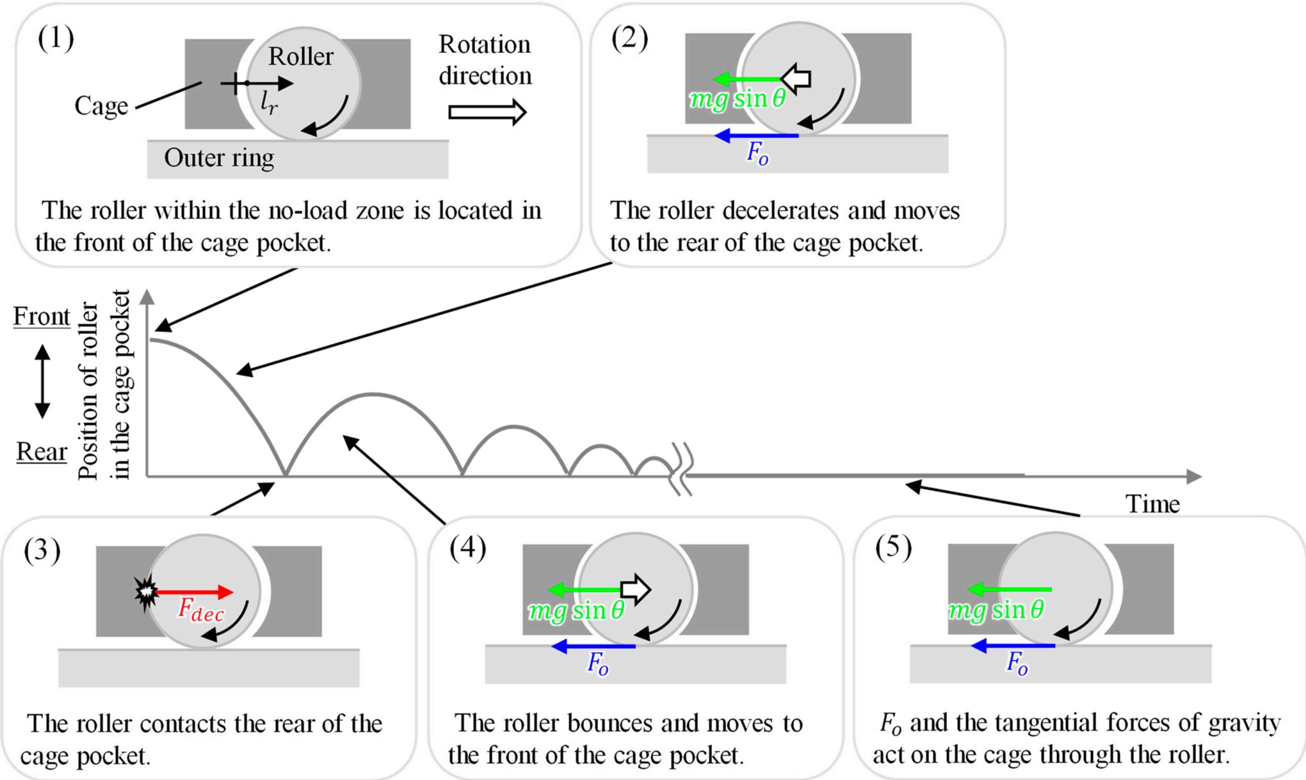


**Figure 4.** Movement of roller in cage pocket.

Thereafter, (2)–(4) are repeated, and the relative velocity between the roller and the cage vanishes.

(5) When the relative velocity between the roller and the cage is zero, $F_o$ and the tangential forces of gravity act on the cage through the roller.

The roller motion shown in Figure 4 is formulated as follows. The equation of motion of the roller is expressed by Equation (1)

$$m\frac{d^2 l_r}{dt^2} = F_{dec} - F_o - mg\sin\theta \tag{1}$$

where $l_r$ is the position of the roller in the cage pocket shown in Figure 4. $F_o$ is given by Equation (2), which is arranged based on the study of Zhou et al. [25].

$$F_o = cN^{0.246}V^{0.648} \tag{2}$$

where $c$ is a constant, $N$ is the normal force between the roller and the outer ring, and $V$ is the rolling velocity between the roller and the outer ring. $N$ is the sum of the centrifugal force and the normal force of gravity acting on the roller, and is given by Equation (3).

$$N = mr_p{\omega_c}^2 + mg\cos\theta \tag{3}$$

$V$ is given by Equation (4).

$$V = \frac{r_r|\omega_r| + r_o\omega_c}{2} \tag{4}$$

$F_{dec}$ is given by Equation (5).

$$\int F_{dec}dt = mv' - mv \tag{5}$$

where $v$ is the relative velocity of the roller and the cage before contact, and $v'$ is the relative velocity of the roller and the cage after contact. Equation (5) can be rewritten as Equation (6) by introducing the coefficient of repulsion between the roller and the cage $e$ $(= |v\prime/v|)$.

$$\int F_{dec}dt = -m(1+e)v \tag{6}$$

Equations (1)–(6) are used to obtain the motion of the roller. $dl_r/dt$ and $l_r$ were obtained by discretizing using a finite difference method as shown in Equations (7) and (8).

$$v_{n+1} = \begin{cases} -\frac{1}{m}(F_o + mg\sin\theta)\Delta t + v_n & l_r \neq 0 \\ -ev_n & l_r = 0 \end{cases} \tag{7}$$

$$l_{n+1} = v_{n+1}\Delta t + l_n \tag{8}$$

where $v_n$ and $l_n$ are the discretized $n$-th $dl_r/dt$ and $l_r$, respectively, and $\Delta t$ is the time increment. The cases were divided based on $l_r$ and $dl_r/dt$, and $I_{dec}$ was determined using Equation (9).

$$I_{dec} = \begin{cases} 0 & l_r \neq 0 \\ \int F_{dec}dt = -m(1+e)v & l_r = 0 \cap \frac{dl_r}{dt} < 0 \\ \int (mg\sin\theta + F_o)dt & l_r = 0 \cap \frac{dl_r}{dt} = 0 \end{cases} \tag{9}$$

Using the method described above, $l_r$, $dl_r/dt$, and $I_{dec}$ were obtained. When $n_i$ is changed, $\omega_i$, $\omega_c$, $\omega_r$, and $\theta$ also change as shown in Equation (10) through (13).

$$\omega_i = 2\pi\frac{n_i}{60} \tag{10}$$

$$\omega_c = \frac{(1-\gamma)\omega_i}{2} \tag{11}$$

$$\omega_r = \frac{(1/\gamma-\gamma)\omega_i}{2} \tag{12}$$

$$\theta = \omega_c t + \phi \tag{13}$$

To perform the calculation in the no-load zone, the initial $\theta$ was set to half the angle of the load zone $\phi$, and the final $\theta$ was set to 23.5 $^\circ - \phi$. $\phi$ is 23.5 $^\circ$, which was calculated by assuming that the load acting on the bearing was 970 N. The initial $l_r$ was defined as the diameter difference between the cage pocket and the roller. $c$ was determined by trial and error. $e$ was set to 0.8 with reference to a paper [26] that measured the $e$ of brass.

## 3. Results and Discussion

### 3.1. Comparison of Measurement and Dynamic Analysis

An example of the measurement results is shown in Figure 5. $F_c$ are shown for one rotation of the cage, starting at the center of the no-load zone. $F_{acc}$ was generated continuously within the load zone. On the other hand, $F_{dec}$ was generated intermittently in the no-load zone and was more impactful than $F_{acc}$. These trends were almost the same even at different rotational speeds. In summary, $F_c$ have the following characteristics.

(a) Force to accelerate the cage $F_{acc}$

$F_{acc}$ occurs continuously from the center of the load zone to the exit. This force is generated by the roller and accelerated by the traction from the inner and outer rings in the load zone pushing against the cage.

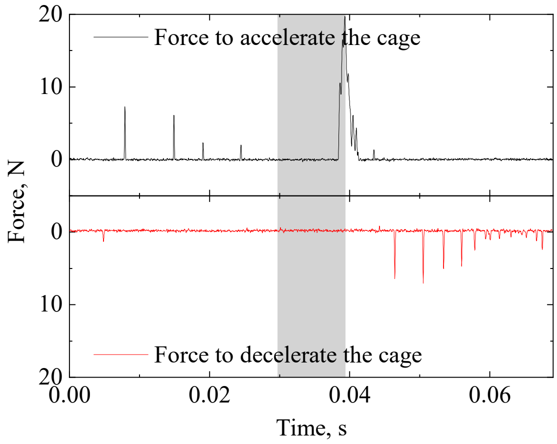


**Figure 5.** Example of measured contact force between roller and cage (2000 rpm, Forward).

(b) Force to decelerate the cage $F_{dec}$

$F_{dec}$ occurs intermittently from the entrance of the no-load zone. This force is generated when the roller is decelerated by the pressure force from the oil film on the outer ring and impacts the cage. The roller is accelerated by impacting the cage, but is decelerated by the pressure force, so it impacts the cage again. The repetition of such impacts continues until the roller and the cage reach the same speed or the roller escapes the no-load zone.

The measurements show that $F_c$ are intermittent forces. Of these, $F_{dec}$ is impact force. Therefore, the volume of cage wear $V_w$ due to such intermittent force is considered. It is known that $V_w$ under constant force contact follows the following equation proposed by Archard [22];

$$V_w = k\frac{WL_s}{H} \tag{14}$$

where $k$ is the coefficient of wear, $W$ is the contact force of two objects, $L_s$ is the sliding distance, and $H$ is the hardness of softer material in two contact materials. On the other hand, it is known that $V_w$ under impact force contact follows the following equation proposed by Lewis [27];

$$V_w = k\frac{WL_s}{H} + K{e_k}^n \tag{15}$$

where $K$ is the coefficient of impact wear, $e_k$ is the kinetic energy at contact, and $n$ is the coefficient of impact wear. Equation (15) shows $V_w$ per contact, where the first term represents sliding wear during contact and the second term represents impact wear. The second term in Equation (15) is ignored, as it is the same as in Equation (14). In this paper, as in the previous paper [21], the second term in Equation (15) is ignored and $V_w$ is considered as following Equation (14). The necessity of the second term in Equation (15) is discussed later. From Equation (14), $V_w$ is proportional to the product of $W$ and $L_s$. In the case of contact between the roller and cage, the $F_c$ shown in Figure 5 is not constant, so $WL_s$ is obtained by integrating $F_c$ with $L_s$. In addition, $L_s$ is given by the product of the time $t$ and the surface velocity of the roller $r_r\omega_r$. From these, $WL_s$ is given by Equation (16).

$$WL_s = \int F_c dL_s = \int F_c dt \cdot r_r\omega_r = I_c \cdot r_r\omega_r \tag{16}$$

where $I_c$ is the impulse caused by $F_c$. Since $r_r$ can be regarded as a constant, from Equations (14) and (16), $V_w$ is proportional to the product of $I_c$ and $\omega_r$. Therefore, finding $I_c$ per cage rotation could be an index to evaluate $V_w$. $I_c$ per cage rotation corresponds to the area obtained by integrating the $F_c$-$t$ graph shown in Figure 5. An example of the results obtained for $I_c$ is shown in Figure 6. Here, for $F_{acc}$, the integration is started from the entrance of the load zone, since it is mainly generated in the load zone, and for $F_{dec}$, the integration is started from the entrance of the no-load zone, since it is mainly generated in the no-load zone. Let $I_{acc}$ be the impulse obtained by integrating $F_{acc}$ with $t$ and $I_{dec}$ be the impulse obtained by integrating $F_{dec}$ with $t$. In the figure, the cumulative value of $I_c$ for one cage rotation from the start of integration is shown for 100 cage rotations. $I_{acc}$ increases significantly in the load zone and does not change much in the no-load zone. $I_{acc}$ may increase significantly within the load zone or not much. This is because the acceleration of the cage by $F_{acc}$ occurs when the cage is decelerated to some degree by $F_{dec}$, which does not happen every time. On the other hand, $I_{dec}$ gradually increases and saturates from the entrance of the no-load zone. $I_{dec}$ follows approximately the same transition for each cage rotation.

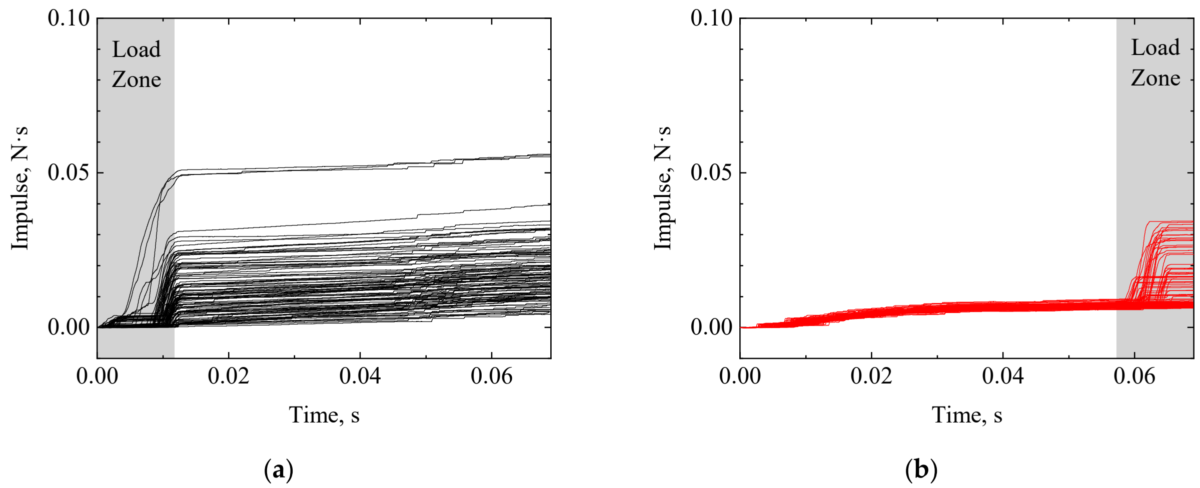


**Figure 6.** Impulse by contact force between roller and cage. (**a**) by force to accelerate the cage (**b**) by force to decelerate the cage (2000 rpm, Forward, Data for 100 cage rotations).

As shown in Figure 6, $I_c$ can be obtained by integrating $F_c$ with $t$. The results of $I_c$ per cage rotation under the conditions shown in Table 2 are shown in Figure 7. Here, the value at each $n_i$ represents the average value for 100 cage rotations, and the error bars indicate the standard deviation. The rotational direction of the inner ring was tested in both forward and reverse, and the results are shown for each. $I_c$ shows almost the same value whether the rotation direction is forward or reverse. This is because the same phenomenon is observed regardless of the direction of rotation, indicating that the measurement was properly performed. $I_{acc}$ and $I_{dec}$ per cage rotation have approximately the same value if $n_i$ is the same. This is because when the cage is rotating at a constant rotational speed, the work by $F_{acc}$ on the cage and the work by $F_{dec}$ on the cage are balanced when considered over a sufficiently long time. However, when considered over a short time, $I_{acc}$ per cage rotation has a large standard deviation because $F_{acc}$ does not occur every rotation. It is shown that $F_{acc}$ only occurs when the rotation of the cage is slowed down to some degree by $F_{dec}$. On the other hand, $I_{dec}$ per cage rotation has a small standard deviation because the roller impact on the cage in the no-load zone is a highly reproducible phenomenon. $I_{acc}$ and $I_{dec}$ per cage rotation become smaller as $n_i$ increases, and do not change much as $n_i$ exceeds 2000 rpm.

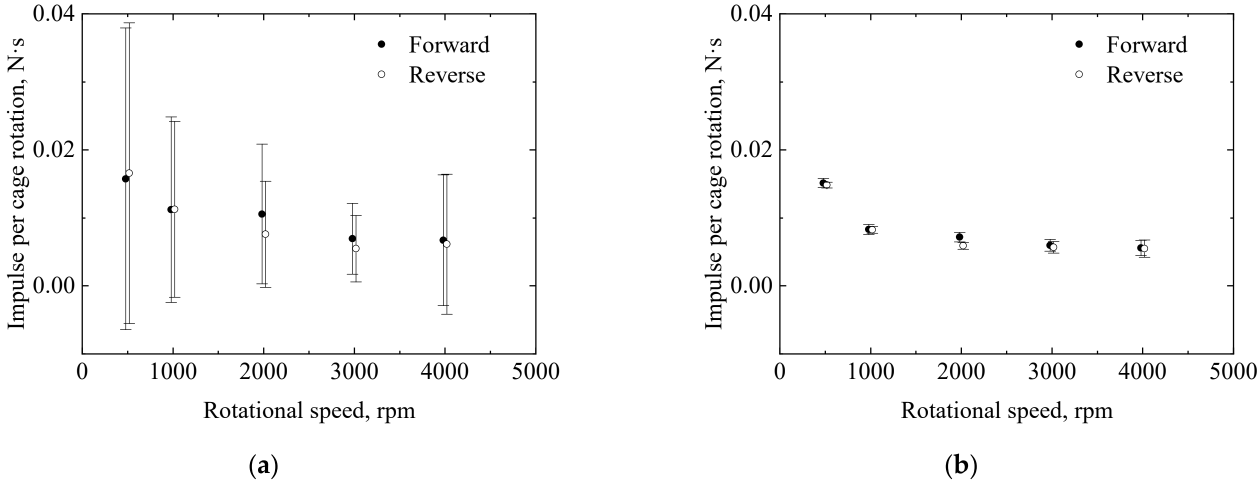


**Figure 7.** Impulse by contact force between roller and cage at each rotational speed [21]. (**a**) By force to accelerate the cage; (**b**) by force to decelerate the cage (average and standard deviation for 100 cage rotations).

The dynamic analysis was performed and the calculation results were compared with the measurement results shown in Figure 7(b). The analysis conditions were the same as for the measurements, with the addition of 5000 and 6000 rpm to $n_i$. Examples of the calculation results for $I_c$, $dl_r/dt$, and $I_{dec}$ are shown in Figure 8. Here, are the results of the calculation for one rotation of the cage (without load zone) when $n_i$ is 3000 rpm, and $c$ is 0.02. The roller repeatedly contacts the rear of the cage pocket. These contacts increase the cumulative total of $I_{dec}$ in a staircase fashion.

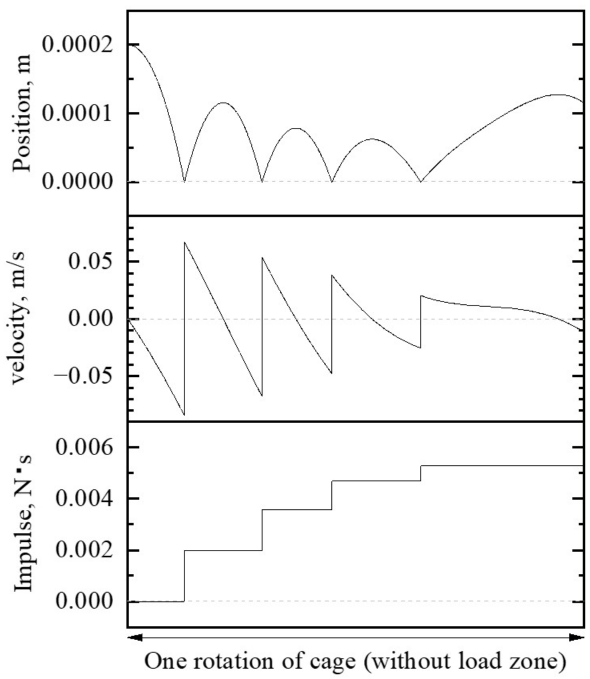


**Figure 8.** Calculation results for position, velocity, and impulse of roller (3000 rpm).

The calculation results of $I_{dec}$ per cage rotation for each of the conditions are shown in Figure 9. The measurement results of $I_{dec}$ per cage rotation shown in Figure 7b are also shown here. In the figure, calculation results are shown for $c$ of 0.01, 0.02, and 0.03. When $c$ is 0.02, the calculation and the measurement results are almost identical. The results for when $c$ is 0.02 in the previous report [21] are also shown, which differ from the present calculation results when $n_i$ is less than 1000 rpm. This indicates that adding "the gravity acting on the rollers" and "the interaction between the roller and the cage when they are at the same speed" to the previous analytical model improved the accuracy of the dynamic analysis. Even under the conditions of 5000 and 6000 rpm for $n_i$, where no measurement results are available, the calculation results show that $I_{dec}$ is almost the same as in the case of 4000 rpm. $I_{dec}$ at each. when $c$ is 0.02 are shown in Figure 10. The measurement results of $I_{dec}$ at all $n_i$ are also shown here. Because of the small variation in measurement results for $I_{dec}$ per cage rotation, $I_{dec}$ is shown here for one representative rotation. In the calculation and measurement, not only the value of $I_{dec}$ per cage rotation, but also the change in $I_{dec}$ during cage rotation is in good agreement with accuracy. Based on this, the proposed method can obtain $I_{dec}$ per cage rotation with good accuracy.

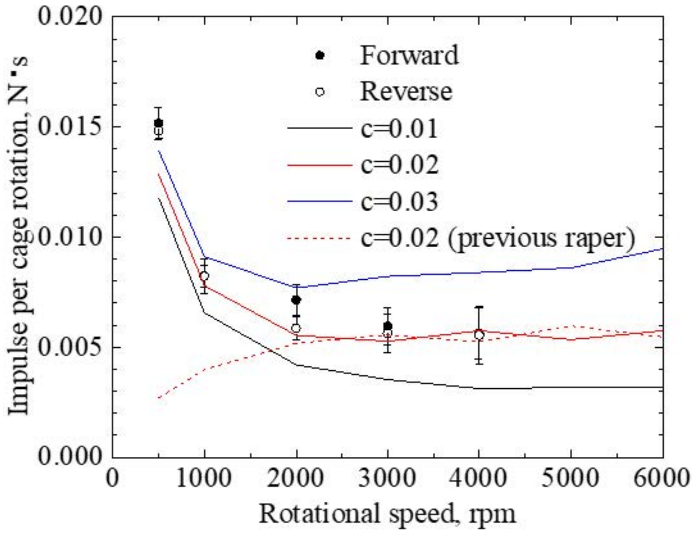


**Figure 9.** Calculation results for impulses per cage rotation.

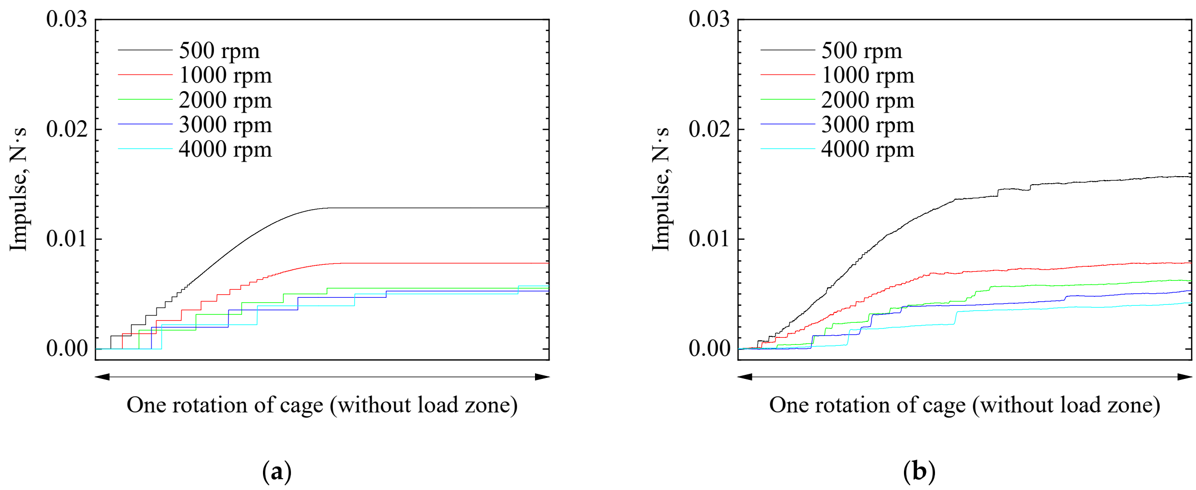


**Figure 10.** Impulse by contact force between roller and cage at each rotational speed. (**a**) Calculation results; (**b**) measurement results.

### *3.2. Determining Wear Modes*

The discussion in this paper has been based on the assumption that cage wear is proportional to the impulse caused by the contact between the roller and the cage, as shown in Equation (16). Here, it is experimentally ascertained whether cage wear obeys this assumption. If the cage wear is in accordance with Equation (16), $V_w$ is considered to be equal for the same value of $I_c$ regardless of the contact force, contact time, or contact frequency between the roller and the cage. As shown in Figure 5, $F_{acc}$ and $F_{dec}$ differed in their contact force, contact time, and contact frequency. On the other hand, as shown in Figure 7, $I_{acc}$ and $I_{dec}$ per cage rotation were almost identical. If cage wear follows Equation (16), the wear at the front of the cage pocket where $F_{acc}$ acts should be equal to the wear at the rear of the cage pocket where $F_{dec}$ acts. Impact wear is also mentioned, and the possibility that cage wear follows Equation (15) proposed by Lewis is also shown. If cage wear is impact wear, for the same value of $I_c$, $V_w$ is expected to increase as the number of contacts increases. In other words, the rear of the cage pocket, where more intermittent $F_{dec}$ acts, should wear more than the front of the cage pocket, where $F_{acc}$ acts.

Based on the above, by measuring cage wear when the bearing is rotated in one direction, it is possible to verify what mode of wear the cage is. That is, if the wear in the rear of the cage pocket is greater than that in the front of the cage pocket, cage wear should be considered impact wear; if the two are approximately equal, cage wear follows the assumptions of this paper. Therefore, an experiment was conducted in which the bearing was rotated in one direction to wear the cage. At the end of the experiment, the volume of wear was measured in the front of the cage pockets and in the rear of the cage pockets. The experimental conditions are shown in Table 3. The dynamic analysis showed that the $I_{dec}$ per cage rotation was almost the same when $n_i$ is 4000 and 6000 rpm. Therefore, to accelerate the test, an experiment was conducted at 6000 rpm. The bearing load was set at 922 N. These conditions were determined with reference to the conditions of use of traction motors for railway vehicles. The test bearing was filled with 0.1 g of grease, which is 1% of the specified amount, to promote cage wear. The temperature of the outer ring of the bearing and the vibration acceleration of the bearing were measured during the experiment. Experiments were conducted until the bearing seized and temperature of the outer ring reached 90 °C.

**Table 3.** Experimental conditions to wear cage.

| | |
|---|---|
| Rotational speed of inner ring $n_i$ | 6000 rpm |
| Rotational direction of inner ring | Forward |
| Radial load | 922 N |
| Lubricant | Lithium complex soap grease<br>0.1 g |

The vibration acceleration of the bearing and the temperature of the outer ring measured during the experiment are shown in Figure 11. Here, acceleration is shown in RMS values. The acceleration and the temperature increased when the total number of rotations exceeded $1.6 \times 10^5$, so the experiment was terminated when the temperature reached 90 °C. The bearing after the experiment is shown in Figure 12. The bearing was seized with cage wear, and wear occurred on either side of the cage pockets. In addition, any of the surfaces of the cage pockets were considered to be adhesive wear. Since adhesive wear was observed in the cage pockets after the test and the contact area between the rollers and the cage is prone to poor lubrication with grease lubrication [28], the contact area between the rollers and the cage was likely in direct contact during the test. The wear shapes were measured for all 16 pockets of the cage using a contact-type profilometer, from which the volume of cage wear was calculated. Each cage pocket was numbered, and the wear shape of pocket 1 is shown as an example in Figure 13. The wear shape of the cage pockets was measured at five locations, 2 mm each in the axial direction. On either side of the cage pocket, the wear shapes were approximately the same in the axial direction. Additionally, wear tended to be greater on the inside and outside of the cage. These features were also observed in other cage pockets. The volume of wear in each pocket was calculated from these wear shapes and the results are shown in Figure 14. Although the volume of wear varied from each cage pocket, within the same pocket, the volume of wear was similar between the front and rear of the cage pocket. When the sum of the volume of wear for the 16 pockets was calculated for the front and the rear of the cage pocket, the two values were approximately the same.

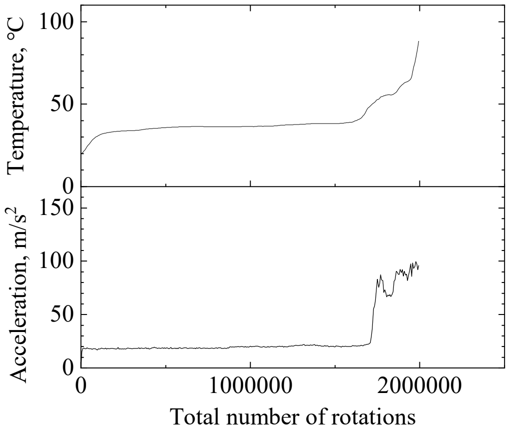


**Figure 11.** Bearing temperature and vibration acceleration during experiment.

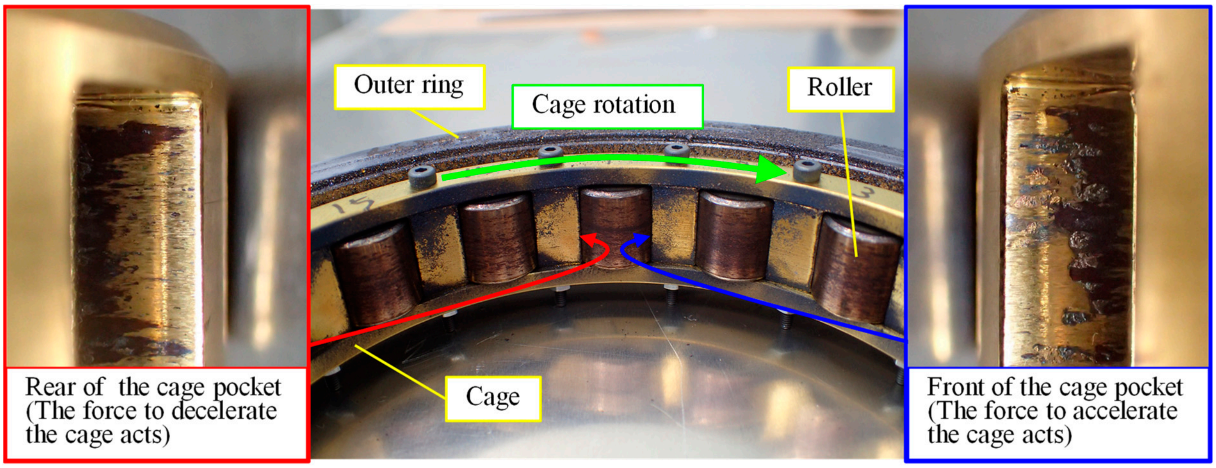


**Figure 12.** Observation of bearing after experiment.

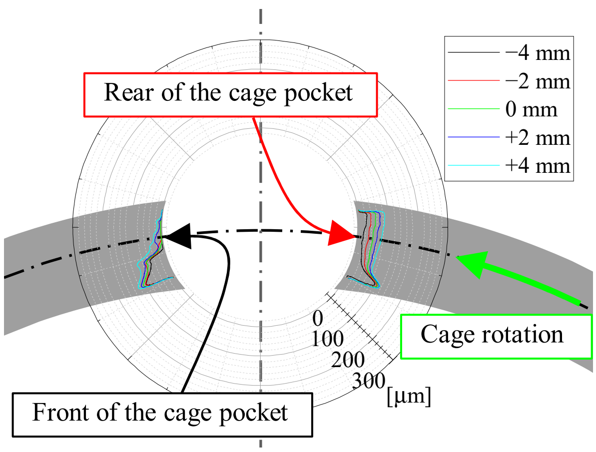


**Figure 13.** Wear shape of cage pocket (pocket 1).

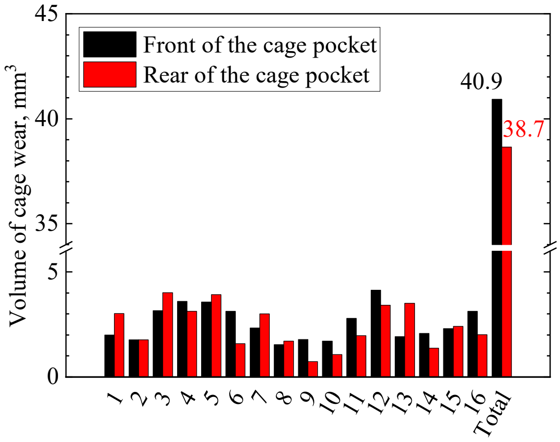


**Figure 14.** Volume of wear in each pocket.

The volume of wear was almost equal in the front of the cage pocket where $F_{acc}$ acts and in the rear of the cage pocket where $F_{dec}$ acts. From this, it can be concluded that cage wear follows Equation (16). Then, the reason why impact wear does not need to be considered in cage wear is discussed. $e_k$ in the present experiment is compared with $e_k$ under the conditions of the paper in which impact wear was formulated. In obtaining $e_k$, it is necessary to determine the impact velocity of the roller and the cage, but since actual measurement is difficult, the dynamic analysis proposed in this paper was used to determine the impact velocity when $n_i$ is 6000 rpm. The result of this calculation is shown in Figure 15. Figure 15 shows the same format as Figure 8. The impact velocity between the roller and the cage is the greatest for the first impact in the no-load zone at 0.112 m/s. From the above, the calculated values of $e_k$ in the present experiment and $e_k$ under the conditions of the paper in which impact wear was formulated are shown in Table 4. The table also shows the values used to calculate $e_k$. $e_k$ in the present experiment is less than one-tenth of $e_k$ under the conditions of the paper in which impact wear was formulated. Since $e_k$ due to contact between the roller and the cage is sufficiently small and the second term in Equation (15) is negligible compared to the first term, impact wear need not be considered in cage wear.

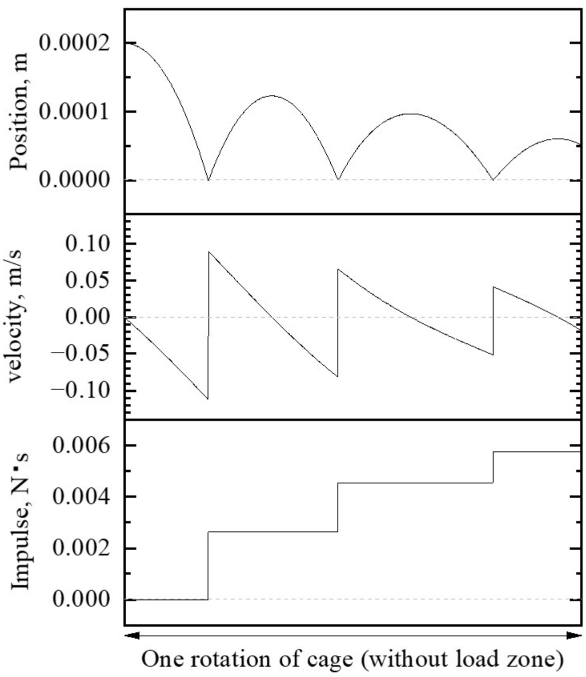


**Figure 15.** Calculated impact velocity of roller and cage (6000 rpm).

**Table 4.** Comparison of kinetic energy of impact.

| | Data for This Paper | Data for Reference [27] |
|---|---|---|
| Mass (Kg) | 0.013 | 0.00055 |
| Impact velocity (m/s) | 0.112 | 2.16 |
| Kinetic energy of impact $e_k$ (J) | $8.15 \times 10^{-5}$ | $1.28 \times 10^{-3}$ |

## 4. Conclusions

The discussion of cage wear was based on the roller motion analysis for cylindrical roller bearings used in traction motors for railway vehicles. As a result, the following findings were obtained:

1. The volume of cage wear is considered to be proportional to the impulse caused by contact, so a method was proposed to calculate this impulse. In this method, a model consisting only of a roller and a cage was constructed, and the movement of the roller relative to the cage was calculated. Using this method, the impulse caused by the contact was determined and compared with the measured results. The calculated results of the impulse were in close agreement with the measured values. Based on this, the analysis model in this paper is reasonable.
2. The experiment was conducted to determine the wear mode of the cage. The results showed that the volume of cage wear is equal when the sum of the impulse is the same, regardless of the magnitude and frequency of the contact forces. In other words, the assumption that cage wear is proportional to the impulse is valid.

In summary, this paper has established a simple method for determining the impulse caused by contact which determines cage wear. This method can be used to predict cage wear and to determine bearing specifications that reduce cage wear.

**Author Contributions:** Conceptualization, D.S. and K.T.; methodology, D.S., K.T., F.I. and S.M.; software, D.S.; validation, D.S. and K.T.; formal analysis, D.S., K.T., F.I. and S.M.; investigation, D.S. and K.T.; resources, D.S. and K.T.; data curation, D.S. and K.T.; writing—original draft preparation, D.S.; writing—review and editing, D.S., K.T., F.I. and S.M.; visualization, D.S.; supervision, F.I.; project administration, D.S. All authors have read and agreed to the published version of the manuscript.

**Funding:** This research received no external funding.

**Data Availability Statement:** The data presented in this study are available on request from the corresponding author.

**Conflicts of Interest:** The authors declare no conflict of interest.

## Nomenclature

| | |
|---|---|
| $r_r$ | radius of roller (m) |
| $r_p$ | pitch circle radius of roller (m) |
| $r_o$ | inner radius of outer ring (m) |
| $m$ | mass of roller (kg) |
| $F_c$ | contact force between roller and cage (N) |
| $F_{acc}$ | $F_c$ to accelerate cage (N) |
| $F_{dec}$ | $F_c$ to decelerate cage (N) |
| $n_i$ | rotational speed of inner ring (rpm) |
| $V_w$ | volume of cage wear ($m^3$) |
| $k$ | coefficient of wear |
| $W$ | contact force of two objects (N) |
| $L_s$ | sliding distance (m) |

| | |
|---|---|
| $H$ | hardness of softer material in two contact materials |
| $K$ | coefficient of impact wear |
| $e_k$ | kinetic energy at impact (J) |
| $n$ | coefficient of impact wear |
| $t$ | time (s) |
| $I_c$ | impulse caused by $F_c$ (=$\int F_c dt$) (N·s) |
| $I_{acc}$ | impulse caused by $F_{acc}$ (=$\int F_{acc} dt$) (N·s) |
| $I_{dec}$ | impulse caused by $F_{dec}$ (=$\int F_{dec} dt$) (N·s) |
| $l_r$ | position of roller in cage pocket (m) |
| $F_o$ | pressure force exerted by oil film between roller and outer ring (N) |
| $N$ | normal force between roller and outer ring (N) |
| $V$ | rolling velocity (m/s) |
| $\gamma$ | $r_r/r_p$ |
| $\omega_i$ | angular velocity of inner ring (rad/s) |
| $\omega_r$ | angular velocity of roller (=$(1-\gamma)\omega_i/2$)) (rad/s) |
| $\omega_c$ | angular velocity of cage (=$(1/\gamma-\gamma)\omega_i/2$) (rad/s) |
| $c$ | constant in Equation (2) |
| $v$ | relative velocity of roller and cage before contact (m/s) |
| $v'$ | relative velocity of roller and cage after contact (m/s) |
| $e$ | coefficient of restitution between roller and cage (=$\lvert v'/v \rvert$) |
| $\phi$ | half angle of load zone (°) |
| $\theta$ | angle of rotation (°) |
| $g$ | acceleration of gravity (m/s$^2$) |

## References


1. Anderson, W.J.; Macka, E.F.; Nemeth, Z.N. Comparison of Performance of Experimental and Conventional Cage Designs and Materials for 75-Millimeter-Bore Cylindrical Roller Bearings at High Speed. U.S. Patent NACA-TR-1177, 1 January 1954.
2. Wagner, F.C.; Burwell, J.T., Jr. New Retainer materials for Aircraft Gas Turbine Bearings. *ASLE Trans.* **1958**, *1*, 1–9. [CrossRef]
3. Wen, B.; Wang, M.; Zhang, J.; Sun, W. Experimental Investigation of Clearance Influences on Cage Motion and Wear in Ball Bearings. *Appl. Sci.* **2021**, *11*, 11848. [CrossRef]
4. Wen, B.; Li, Y.; Wang, M.; Yang, Y. Measurement for Lubricant Distribution in an Angular Contact Ball Bearing and Its Influence Investigation. *Lubricants* **2023**, *11*, 63. [CrossRef]
5. Chen, C.; Deng, Z.; Wang, H.; He, T. Simulation of Friction Fault of Lightly Loaded Flywheel Bearing Cage and Its Fault Characteristics. *Sensors* **2022**, *22*, 8346. [CrossRef]
6. Kudelina, K.; Baraškova, T.; Shirokova, V.; Vaimann, T.; Rassõlkin, A. Fault Detecting Accuracy of Mechanical Damages in Rolling Bearings. *Machines* **2022**, *10*, 86. [CrossRef]
7. Pan, C.; Wang, C.; Zhao, Y.; Cao, G. Study on design and simulation of a novel isolator cylindrical roller bearing. *J. Mech. Sci. Technol.* **2022**, *36*, 3851–3862. [CrossRef]
8. Lundberg, G.; Palmgren, A. Dynamic Capacity of Rolling Bearings. *J. Appl. Mech.* **1949**, *16*, 165–172. [CrossRef]
9. Kakuta, K. The Effects of Misalignment on the Forces Acting on the Retainer of Ball Bearings. *J. Fluids Eng.* **1964**, *86*, 449–454. [CrossRef]
10. Stacke, L.-E.; Fritzson, D. Dynamic behaviour of rolling bearings: Simulations and experiments. *Proc. Inst. Mech. Eng. Part J. J. Eng. Tribol.* **2001**, *215*, 499–508. [CrossRef]
11. Tada, S. Dynamic Analysis of Sound, Vibration and Motion of Cage in High Speed Ball Bearings. *KOYO Eng. J.* **2002**, *160*, 29–36.
12. Chen, S.; Chen, X.; Li, Q.; Gu, J. Experimental Study on Cage Dynamic Characteristics of Angular Contact Ball Bearing in Acceleration and Deceleration Process. *Tribol. Trans.* **2021**, *64*, 42–52. [CrossRef]
13. Gupta, P.K. Dynamics of Rolling-Element Bearings Part I: Cylindrical Roller Bearing Analysis. *J. Lubr. Technol.* **1979**, *101*, 293–302. [CrossRef]
14. Gupta, P.K. Dynamics of Rolling-Element Bearings Part II: Cylindrical Roller Bearing Results. *J. Lubr. Technol.* **1979**, *101*, 305–311. [CrossRef]
15. Gupta, P.K. Dynamics of Rolling-Element Bearings Part III: Ball Bearing Analysis. *J. Lubr. Technol.* **1979**, *101*, 312–318. [CrossRef]
16. Gupta, P.K. Dynamics of Rolling-Element Bearings Part IV: Ball Bearing Results. *J. Lubr. Technol.* **1979**, *101*, 319–326. [CrossRef]
17. Sakaguchi, T.; Harada, K. Dynamic Analysis of Cage Behavior in a Tapered Roller Bearing. *J. Tribol.* **2006**, *128*, 604–611. [CrossRef]
18. Sakaguchi, T.; Harada, K. Dynamic Analysis of Cage Stress in Tapered Roller Bearings Using Component-Mode-Synthesis Method. *J. Tribol.* **2009**, *131*, 011102. [CrossRef]
19. Weinzapfel, N.; Sadeghi, F. A discrete element approach for modeling cage flexibility in ball bearing dynamics simulations. *J. Tribol.* **2009**, *131*, 021102. [CrossRef]
20. Ashtekar, A.; Sadeghi, F. A New Approach for Including Cage Flexibility in Dynamic Bearing Models by Using Combined Explicit Finite and Discrete Element Methods. *J. Tribol.* **2012**, *134*, 041502. [CrossRef]

21. Suzuki, D.; Takahashi, K.; Itoigawa, F.; Maegawa, S. Contact forces between roller and cage pocket in cylindrical roller bearings (Consideration based on dynamic behavior between roller and cage). *Trans. JSME* **2022**, *88*, 22-00153. (In Japanese) [CrossRef]
22. Archard, J.F. Contact and Rubbing of Flat Surfaces. *J. Appl. Phys.* **1953**, *24*, 981. [CrossRef]
23. Dahiwal, R.; Thielen, S.; Sauer, B. Modeling and Simulation of Cage Wear in Solid-Lubricated Rolling Bearings. *Tribol. Online* **2020**, *15*, 25–35. [CrossRef]
24. Gao, S.; Han, Q.; Zhou, N.; Zhang, F.; Yang, Z.; Chatterton, S.; Pennacchi, P. Dynamic and wear characteristics of self-lubricating bearing cage: Effects of cage pocket shape. *Nonlinear Dyn.* **2022**, *110*, 177–200. [CrossRef]
25. Zhou, R.S.; Hoeprich, M.R. Torque of tapered roller bearings. *J. Tribol.* **1991**, *113*, 590–597. [CrossRef]
26. Tatara, Y.; Moriwaki, N. Study on Impact of Equivalent Two Bodies: Coefficients of Restitution of Spheres of Brass, Lead, Glass, Porcelain and Agate, and the Material Properties. *Bull. JSME* **1982**, *25*, 631–637. [CrossRef]
27. Lewis, R. A modelling technique for predicting compound impact wear. *Wear* **2007**, *262*, 1516–1521. [CrossRef]
28. Komoriya, T.; Ichimura, R.; Kochi, T.; Yoshihara, M.; Sakai, M.; Dong, D.; Kimura, Y. Service Life of Lubricating Grease in Ball Bearings (Part 1) Behavior of Grease and Its Base Oil in a Ball Bearing. *Tribol. Online* **2021**, *16*, 236–245. [CrossRef]